# Journal of Applied Sciences

ISSN 1812-5654

science alert

ANSInet
an open access publisher
http://ansinet.com

Journal of Applied Sciences 11 (9): 1587-1593, 2011
ISSN 1812-5654 / DOI: 10.3923/jas.2011.1587.1593


# Model of Neural Networks with Sigmoid and Radial Basis Functions for Velocity-field Reconstruction in Fluid-structure Interaction Problem

[1,2]Mas Irfan P. Hidayat and [1]Bambang Ariwahjoedi
[1]Department of Mechanical Engineering, Universiti Teknologi PETRONAS,
Bandar Seri Iskandar, 31750 Tronoh, Perak Darul Ridzuan, Malaysia
[2]Faculty of Industrial Technology, Institute Teknologi Sepuluh Nopember,
Kampus ITS Keputih Sukolilo, 61111, East Java, Indonesia

**Abstract:** This study presents numerical simulation of velocity-field reconstruction in Fluid-structure Interaction (FSI) problem with the presence of a very step velocity jump at the fluid-solid interface. Models of Neural Network (NN) with sigmoid and radial basis functions were developed and utilized as approaches of investigation to fully reconstruct the velocity-field at the fluid-structure interface of the problem. As a numerical case, one-dimensional compressible fluid coupled with elastic solid under strong impact was simulated. This class of problem belongs to an Eulerian-Lagrangian Riemann problem in which the very step jump of velocity vector does exist. The resolution of the NN models in the vicinity of the interface was further investigated and analyzed in which the accuracy of the NN approach was validated to the problem analytical solution. From the results of the numerical study, high numerical accuracy of the NN models can be obtained in relation with the increase of the interface resolution through which useful insights of this study were also revealed.

**Key words:** Velocity-field reconstruction, fluid-structure interaction, neural network, sigmoid and radial basis functions

## INTRODUCTION

Full characterization of velocity-field in the problems of computational dynamics and Fluid-structure Interaction (FSI) is of paramount importance to visualize the flow dynamics and to achieve the flow-field spatial and time-dependent solution with high accuracy.

Among several applications (Pruvost *et al*., 2000; Pruvost *et al*., 2001; Venturi and Karniadakis, 2004; Pastur *et al*., 2008) velocity-field reconstruction in FSI problem with the presence of velocity vector jump at the fluid-structure interface is of high interest. The condition may be represented in many engineering interests such as the case of a shock in the fluid impacting a nearby solid structure or a solid projectile impacting a fluid (Deshpande *et al*., 2006; Rajendran and Narasimhan, 2006). The study of the problem is therefore of importance also from the numerical point of view. It is well-known that the solving of FSI problem is highly centered on the appropriate numerical treatment at the fluid-structure interface in order to successfully obtain a good accuracy in the overall solution. Thus, its numerical simulation and investigation can provide useful insights for the implementation and strategy extension of numerical scheme applied to the FSI problem and other problems of FSI in general.

In the present paper, numerical study of the velocity-field reconstruction with the presence of a very step jump of velocity vector at the interface of fluid and solid is presented. The main motivation and objective of the study is that investigating the solution nature of FSI problem at the fluid-structure interface with an efficient implementation of numerical approach, but insightful.

As a numerical case, one-dimensional compressible fluid coupled with elastic solid under strong impact was simulated. This class of problem belongs to an Eulerian-Lagrangian Riemann problem in which a very step jump of velocity vector does exist. The problem is also well characterized in the sense that its analytical solution is available under certain assumptions of condition (Liu *et al*., 2008), with which the performances and insights of a numerical approach studied can be assessed.

Models of Neural Network (NN) with sigmoid and radial basis functions were developed and utilized as approaches of investigation to fully reconstruct the velocity-field at the fluid-structure interface of the problem. Subsequently, the resolution of the NN models

**Corresponding Author:** Bambang Ariwahjoedi, Department of Mechanical Engineering, Universiti Teknologi PETRONAS, Bandar Seri Iskandar, 31750 Tronoh, Perak Darul Ridzuan, Malaysia

in the vicinity of the interface was further investigated and analyzed in which the accuracy of the NN approach was validated to the analytical solution of the problem. Moreover, the accuracy of the NN models was compared. This study work is related to the work of Liu *et al.* ( 2008), particularly for the analytical solution of the problem considered in this paper.

**The eulerian-lagrangian riemann problem:** The Eulerian-Lagrangian Riemann problem for the one-dimensional fluid-elastic solid coupling with solid under strong impact is described in this section. Not also that only brief description of the problem formulation was presented in this paper. For great details of its analytical treatment and derivation, the readers are directed to (Liu *et al.*, 2008).

The fluid is assumed to locate on the left side of the interface, while the solid is on the right side of the interface. The following Eulerian-Lagrangian system in the vicinity of the interface is considered:

$$\begin{cases} \dfrac{\partial U}{\partial t}+\dfrac{\partial F}{\partial x}=0, \text{with } U\big|_{t=0}=U_l \text{ for } x<x_0 \\ \dfrac{\partial U}{\partial t}+\dfrac{\partial F}{\partial x}=0, \text{with } V\big|_{t=0}=V_r \text{ for } x'<x_0' \end{cases} \quad (1)$$

where, $x_0$ is the interfacial location in the Eulerian system, while its corresponding coordinate in the Lagrangian system is denoted by $x'_0$. $U_l$ and $V_r$ are the constant velocity vectors of the fluid and solid, respectively, representing the initial conditions of the problem. Initially, $x_0$ and $x'_0$ coincide each other. However, once the diaphragm separating the fluid and solid is removed, the interface moves with a new velocity, $u^e_l$. Thus, relation between $x_0$ and $x'_0$ can be written as $x'_0 = x_0 + u^e_l t$, with respect to the fixed Eulerian system. Furthermore, $u^e_l$ is a constant for the Riemann problem considered.

As a result of the strong impact, shock waves are generated in the system (Liu *et al.*, 2008; Inaba and Shepherd, 2008). In addition, pressure and velocity jumps also exist and the density may as well (Housman *et al.*, 2009a, b).

## NN AND SIMULATION METHOD

The two models of NN employed in this study belong to Multilayer Perceptron (MLP) and Radial Basis Functions Neural Network (RBFNN), respectively. The schematics and features of the NN are described in this section.

**Multilayer perceptron:** Figure 1 shows a schematic diagram of the typical MLP with three layers and single output.

The notations in Fig. 1 are: p input sets, L number of elements in input vector, s number of hidden nodes, n the summed up of weighted inputs, a the output of activation function in the corresponding layer, $w^1_{j,i}$ and $b_j{}^1$ input weight and bias (i = 1 to L, j = 1 to s), $w^2_{1,j}$ and $b_o$ layer weight and output bias, and y the MLP output. The layer of hidden nodes and the second layer of output are denoted by superscripts 1 and 2, respectively.

As depicted in Fig. 1, the output estimate *f* realized by the MLP given the training examples can be written as:

$$\hat{f}(p,w)=\sum_{i=1}^{s} w^2_{1,i}\ \tau\left(w^1_{i,j}\,p+b_i\right)+b_o \quad (2)$$

where: $\tau(.)$ is a sigmoid function used in the nodes of hidden layer. A typical logistic function was used in this study:

$$\tau(n) = 1/(1+e^{-n}) \quad (3)$$

For this numerical study purpose, typical objective function was used as shown in (4):

$$?(w)=\sum_{q=1}^{Q}\left[t_q-\hat{f}(p_q;w)\right]^2 \quad (4)$$

where, $p_q$ is the vector of input sets, $t_q$ is the target output and $\hat{f}(p_q;w)$ is the MLP network output and Q is number of observation data in training set. In addition, the Levenberg-Marquardt Back-propagation (BP) algorithm was chosen as the training algorithm with an intention that the network would give proper response or generalize well to new examples never inputted before. The algorithm steps of Levenberg-Marquardt for adjusting the weights over the training examples are described in detail by Hagan *et al.* (1996).

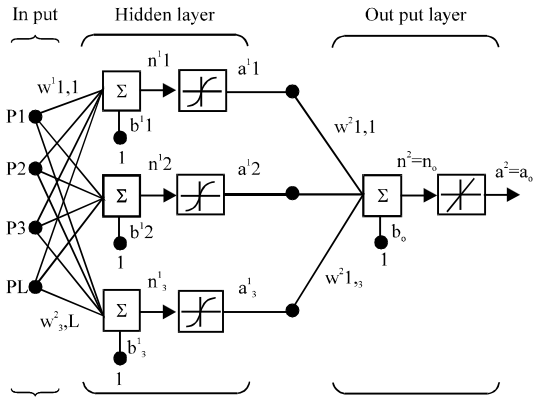


Fig. 1: Schematic diagram of MLP

**Radial basis function neural network:** Figure 2 describes a schematic diagram of the RBFNN with the distance function of Euclidean distance denoted by $\|x-c_i\|$, which will be further explained in this section. In Fig. 2, the input sets are denoted by x, the target outputs are denoted by y and the number of hidden nodes is represented by s.

As depicted in Fig. 2, it is clear that in RBFNN, the connections between the input and the hidden layers are not weighted. The inputs, therefore, reach the hidden layer nodes unchanged. In addition, the output estimate $\hat{f}$ realized by the RBFNN given the training examples can be expressed as:

$$\hat{f} = \sum_{i=1}^{S} \phi_i\left(\|x - c_i\|\right) W_{j,i} \quad (5)$$

where, x is the vector of input sets, $c_i$ is the ith center node in the hidden layer and $w_{j,i}$ is the vector of weights from the output nodes to the center nodes, $\phi_i$ are the radial basis functions of the center nodes, $\|x-c_i\|$ is the distance between the point representing the input x and the center of the ith hidden node as measured by some norm.

In this numerical study, the most widely used radial basis function $\phi$ was employed, namely Gaussian function, as follows:

$$\varphi\left(\|x - c_i\|\right) = \exp\left(-\frac{(\chi-\gamma)^2}{\psi^2}\right) \quad (6)$$

where, $\gamma$ and $\Psi$ are the parameters that control the position and width of the RBF centers, respectively.

From the previous explanation, it is clear that there are four sets of parameters to be determined in the training of the RBFNN. The parameters are governing the network mapping properties, namely the number of centers in the hidden layer, the position of RBF centers, the width of RBFs, and the RBFNN weights.

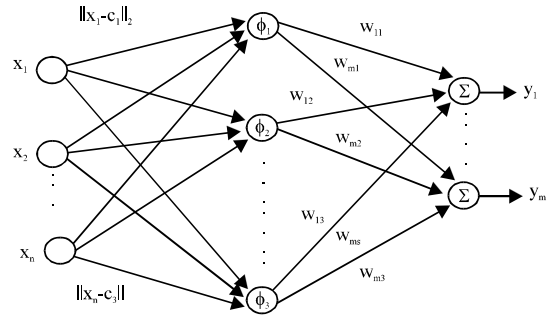


Fig. 2: Schematic diagram of RBFNN

Different with the training of MLP, training of RBFNN involves both supervised and unsupervised learning methods. The output layer is trained by a supervised learning method, similar to that used in the BP algorithm. The synaptic weights are updated as usual with respect to the objective function of (4). On the other hand, training of the hidden layer involves the determination of the first three parameters mentioned. The parameters are dependent only on the inputs and are independent of the outputs, thus making this part of the learning process an unsupervised one. The readers are directed to Haykin (1994) for several procedures of the RBFNN parameters determination.

**Simulation procedures:** In general, learning in NN is achieved by adjusting the corresponding weights w in response to a set of training data presented to the network. The training data consists of pairs of a vector from an input space and a desired network target. Through a set of learning rule or learning algorithm, the error between the actual and desired response or target is minimized with respect to an objective function E(w) relative to some optimization criterion or learning parameters.

The NN model prediction is then achieved by inputting a new data set (testing data set) never presented before to the trained network. The procedures thus allow the full feature of data to be estimated and constructed from the partial data available. This is where the advantage of using NN is lying.

In this research work, the velocity-field data was divided into two sets of training and testing data. The full data was generated from (1) where its analytical solution was available (Liu *et al.*, 2008). In addition, 50% of the full data was used as the training set, while the remaining set as the testing set. The accuracy of the NN models was then analyzed. Programming lines for this numerical study were written in MATLAB environment.

## RESULTS AND DISCUSSION

The simulation results of the velocity-field reconstruction using the NN models for the problem are presented below.

Also, because the problem considered in this numerical study was one-dimensional, it is reasonable to give attention to the variation of the number of data points which could represent the number of measurement points and also to the spatial distribution of data points. It is also important to note that the NN simulation results for the training phase of the NN were not shown in the next following sections. Thus only the results of the NN

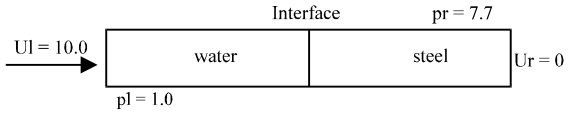


Fig. 3: Schematic diagram of the water-solid Eulerian-lagrangian riemann problem together with the initial conditions

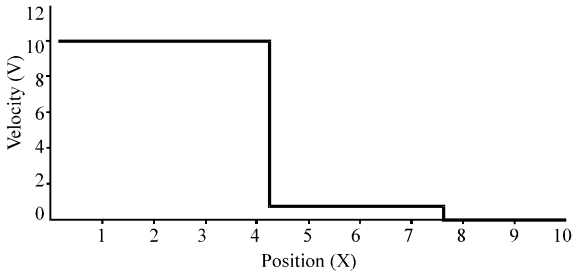


Fig. 4: Analytical solution of the water-solid Eulerian-lagrangian riemann problem considered in this study

simulation with the testing data sets that were shown. The results of simulation performed by the NN models were measured by Means of Squared Error (MSE) value. It is important to note that the MSE values presented was the averaged values from many times simulation running, with a very small variation of the value from the many times running.

The analytical solution from (1) was obtained first by assigning the materials properties of the fluid and solid involved. The fluid was water and the solid was stainless steel of AISI Type 431 with the properties of Poisson ratio 0.283, Young's modulus 215.116 GPa and density 7700 kg $m^{-3}$. The calculation was non-dimensionalized, where the density was non-dimensionalized with 1000 kg $m^{-3}$, and the non-dimensional domain chosen was X = [0, 10] (Liu *et al*., 2008).

Figure 3 shows the schematic of the water-solid Eulerian-Lagrangian Riemann problem considered. The problem initial conditions are: $u_l$ = 10.0, $\rho_l$ = 1.0 and $u_r$ = 0.0, $\rho_r$ = 7.7. Note that the solid is initially at rest, while the fluid is impacting the solid.

Figure 4 plots the analytical solution of the water-solid Eulerian-Lagrangian problem with a shock wave in the water medium.

From Fig. 4, it can be observed clearly the development of the velocity-field along the non-dimensional domain. There are five distinct regions consisting of two sharp jumps of the velocity-field. Note also the very step of velocity vector jump at the water-steel interface.

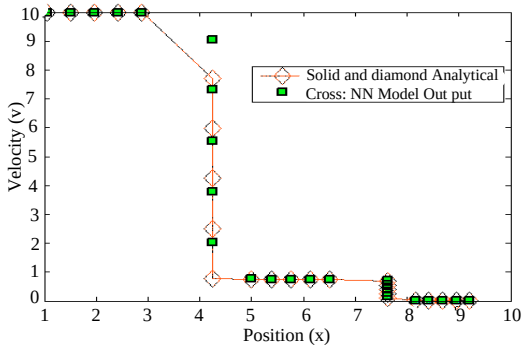


Fig. 5: Velocity-field prediction results using MLP model with 5 data points at the interface

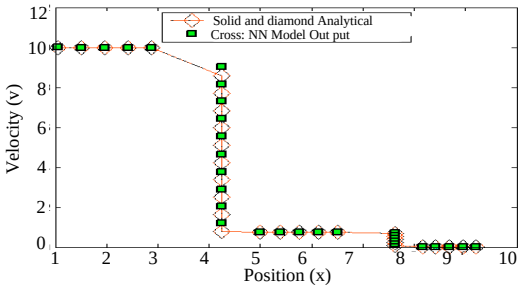


Fig. 6: Velocity-field prediction results using MLP model with resolution of 10 data points at the interface

**The MLP simulation results:** For the MLP model, the number of hidden nodes of 5 was previously set. In addition, the maximum number of iteration was set to 300. Initially, the number of data points of 10 was assigned for each region in Fig. 3 without considering the distinct natures of the regions, and 50% of the data points were used in the training phase of the MLP. Figure 5 shows the simulation results of velocity-field prediction using the MLP model.

It can be seen clearly that there were large discrepancies between the analytical solution and the prediction of MLP model at the water-steel interface, when using the number of data points in the MLP training phase. Meanwhile at other location of velocity vector jump at X = 7.63, the number of data points used seems to be adequate. This may indicate that the resolution at the interface needs to be increased.

Figure 6 depicts the simulation results of velocity-field prediction using the MLP model when the resolution at the interface was increased by using 10 data points.

It can be observed clearly that the MLP velocity-field prediction results were getting better with the increased resolution at the interface, while the number of data points for other locations was kept constant.

Table 1: MSE values of velocity-field prediction results using MLP model with respect to resolutions at the locations of velocity vector jump

| The number of data points at the locations of velocity vector jump | MSE values |
|---|---|
| 5 and 5 | 0.3416 |
| 10 and 5 | 0.0640 |
| 10 and 10 | 0.0558 |
| 20 and 10 | 0.0208 |

Further, it may also be interesting to see the MLP simulation results when the resolutions at the locations of velocity vector jump are further increased. Not only at the interface the number of data points was now increased, but also at other location of velocity vector jump, X = 7.63.

Fig. 7 and 8 show the simulation results of velocity-field prediction using the MLP model when the resolutions at the locations of velocity vector jump are further increased. In Fig. 7, the resolutions are of 10 and 10 data points, respectively, while in Fig. 8 the resolutions are of 20 and 10 data points, respectively. Note that the resolution increase may be not too apparent at the location of X = 7.63.

The MSE values of the velocity-field prediction results using the MLP model were summarized in Table 1.

**The RBFNN simulation results:** For the RBFNN model, the number of hidden nodes of 20 was chosen. In addition, the spread value $\Psi$ between 0.5 and 10 was found to be adequate for the hidden node number. Thus, the spread value was set to 3.

In addition, the numerical strategy used for the RBFNN was similar to that for the MLP, where the resolution points at the velocity vector jump locations were gradually increased and the effect of the resolution increase to the prediction results was subsequently observed.

Figure 9 shows the simulation results of velocity-field prediction using the RBFNN model. The number of data points of 5 for each region in Fig. 3 was used in the RBFNN training phase.

It can be observed that the prediction results of the RBFNN model were similar to those of the MLP model. The large discrepancies between the analytical solution and the prediction of the RBFNN were also observed at the water-steel interface.

Further, for the resolution of 10 data points at the water-steel interface, the prediction results obtained was shown in Fig. 10.

Note again that the prediction results obtained by the RBFNN model were similar to those obtained by the MLP model for the same number of resolution at the interface.

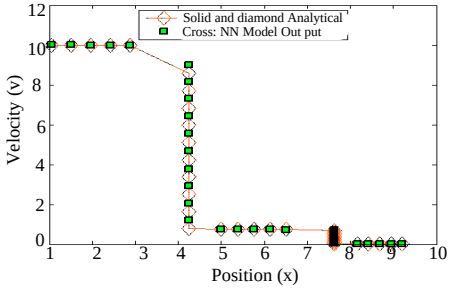


Fig. 7: Velocity-field prediction results using MLP model with resolutions of 10 and 10 data points, respectively at the locations of velocity vector jump

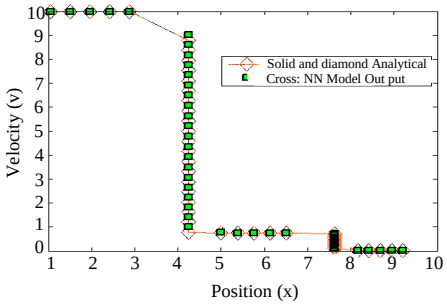


Fig. 8: Velocity-field prediction results using MLP model with resolutions of 20 and 10 data points, respectively at the locations of velocity vector jump

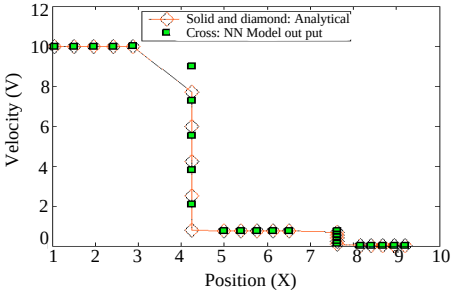


Fig. 9: Velocity-field prediction results using RBFNN model with 5 data points at the interface

In Fig. 11 and 12, the simulation results of velocity-field prediction using the RBFNN were shown for the increase of resolutions at the velocity vector jump locations.

The MSE values of the RBFNN prediction results were shown in Table 2.

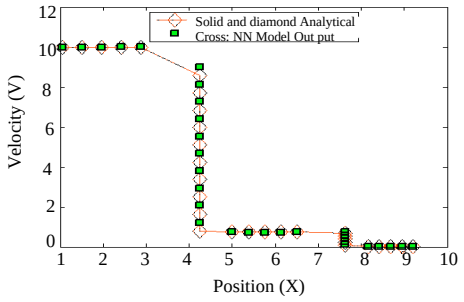


Fig. 10: Velocity-field prediction results using MLP model with resolution of 10 data points at the interface

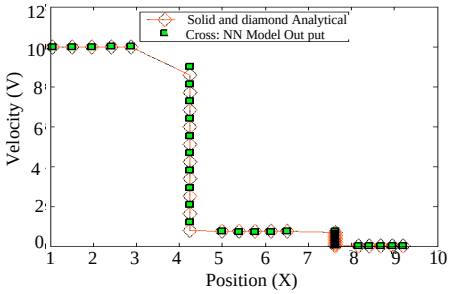


Fig. 11: Velocity-field prediction results using RBFNN model with resolutions of 10 and 10 data points, respectively at the locations of velocity vector jump

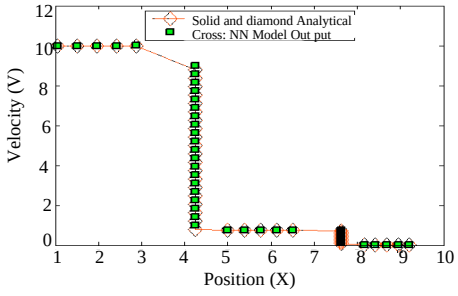


Fig. 12: Velocity-field prediction results using RBFNN model with resolutions of 20 and 10 data points, respectively at the locations of velocity vector jump

**Further discussions:** From the simulation results obtained, it can be said that special attention must be given to the locations where velocity vector jump takes place. To achieve high accuracy for the velocity-field reconstruction, the resolution at the locations of velocity vector jump needs to be increased.

Furthermore, at the location with a very step of velocity jump, the resolution needs to be high. For the problem considered in this study, it was the fluid-solid interface, as can be examined from the corresponding MSE values of the NN prediction results as shown in Table 1 and 2.

Table 2: MSE values of velocity-field prediction results using RBFNN model with respect to resolutions at the locations of velocity vector jump

| The number of data points at the locations of velocity vector jump | MSE values |
|---|---|
| 5 and 5 | 0.3369 |
| 10 and 5 | 0.0627 |
| 10 and 10 | 0.0540 |
| 0 and 10 | 0.0200 |

Table 3: Comparison of the MSE values of the MLP and RBFNN prediction results

| | MSE values | |
|---|---|---|
| The number of data points at the locations of velocity vector jump | MLP | RBFNN |
| 5 and 5 | 0.3416 | 0.3369 |
| 10 and 5 | 0.0640 | 0.0627 |
| 10 and 10 | 0.0558 | 0.0540 |
| 20 and 10 | 0.0208 | 0.0200 |

This also may indicate that for a numerical scheme employed for an FSI problem, the resolution at the fluid-solid interface should be high and fine. In fact, for grid or mesh based numerical methods, such as FEM and particle methods, the mesh or grid employed around the interface is denser or finer than that at other locations in the solution domain to achieve the solution with high accuracy.

Also, from the results of the velocity-field reconstruction, the spatial distribution of the data points is also of importance, besides the number of data points. The spatial distribution of data points describes how the data points distribute along the solution domain and it should represent the regions of interests in the solution domain.

Moreover, the models of NN with sigmoid and radial basis functions employed in this numerical study resulted in comparable MSE values. It is interesting to note, however, that the RBFNN model always give better accuracy for the same number of resolutions used, although more model parameters must be determined for the RBFNN model. This was shown in Table 3.

The better accuracy of the RBFNN model may be attributed to the use of radial basis functions having parameters that control the positions of the RBFs among the data or sample points and also their widths of influence (spread) to the sample points, namely the parameters of $\gamma$ and $\Psi$. The parameters further help the RBFNN model resolution capability, thus in turn leads to better solution accuracy.

Further insight of this is that numerical schemes utilizing or incorporating radial or other basis functions with high resolution capability may become preference of

choice to efficiently model and simulate the FSI problem in general and for the suitable numerical treatment of the fluid-solid interface in particular. In fact, what it is clear is that the use of high number of grid points or mesh such as in typical FEM is not without cost, for examples effort and time for mesh preparation, long running time, especially for more complex problem situations in higher dimensional solution domain of 2 and 3D. To some extent, it might also include convergence and compatibility issues.

## CONCLUSION

The one-dimensional fluid-elastic solid coupling Riemann problem has been simulated and investigated in the present paper as a numerical case for FSI problem considered in this study. Models of NN with sigmoid and radial basis functions have been developed and utilized as approaches of investigation to fully reconstruct the velocity-field at the fluid-structure interface of the problem.

With the presence of a very step velocity jump at the fluid-structure interface of the problem, high numerical accuracy of the NN models can be obtained in relation with the increase of the interface resolution.

In addition, the RBFNN model always gives better accuracy than the MLP model for the same number of data points used at the locations of velocity vector jump. When using resolutions of 20 and 10 data points, the MSE value of the RBFNN prediction result was 0.0200, while that of the MLP prediction result was 0.0208. The RBFNN has also shown representative model having high spatial and resolution capability for the problem considered with the resolution accuracy achieved at the fluid-structure interface.

From the prediction point of view, the capability of the NN models was ensured by the small MSE values. This may have high relevant and important value in particular when limited experimental measurement data are to be utilized for full velocity-field reconstruction.

The use of other numerical scheme with basis functions having high multi-resolution and multi-scale capabilities may be recommended for further numerical treatment and extension for the FSI problem. This would be the subject of further study.

## ACKNOWLEDGMENT

The grant provided by Universiti Teknologi PETRONAS is gratefully acknowledged.

## REFERENCES

Deshpande, V.S., A. Heaver and N.A. Fleck, 2006. An underwater shock simulator. Proc. R. Soc. A 8, 462: 1021-1041.

Hagan, M.T., H.B. Demuth and M. Beale, 1996. Neural Network Design. PWS Publishing Company, Boston, New York, USA.

Haykin, S., 1994. Neural Networks: A Comprehensive Foundation. Macmillian College Publishing Company, New York, ISBN-10: 0023527617.

Housman, J.A., C.C. Kiris and M.M. Hafez, 2009a. Time-derivative preconditioning methods for multicomponent flows-part I: Riemann problems. J. Applied Mech., 76: 1-13.

Housman, J.A., C.C. Kiris and M.M. Hafez, 2009b. Time-derivative preconditioning methods for multicomponent flows-part II: Two-dimensional applications. J. Applied Mech., 76: 1-12.

Inaba, K. and J.E. Shepherd, 2008. Impact generated stress waves and coupled fluid-structure responses. Proceedings of the 11th International Congress and Exposition on Experimental and Applied Mechanics, June 2-5, Orlando, FL, USA., pp: 1-12.

Liu, T.G., J.H. Ho, B.C. Khoo and A.W. Chowdhury, 2008. Numerical Simulation of fluid-structure interaction using modified ghost fluid method and naviers equations. J. Sci. Comput., 36: 45-68.

Pastur, L.R., F. Lusseyran, T.M. Faure, B. Podvin and Y. Fraigneau, 2008. POD based technique for 3D flow reconstruction using 2D Data set. Proceedings of the 13th International Symposium on Flow Visualization (ISFV13), July 1-4, Nice, France, pp: 1-5.

Pruvost, J., J. Legrand and P. Legentilhomme, 2001. Three-dimensional swirl flow velocity-field reconstruction using a neural network with radial basis functions. J. Fluids Eng., 123: 920-927.

Pruvost, J., J. Legrand, P. Legentilhomme and L. Doubliez, 2000. Particle image velocimetry investigation of the flo7w-field of a 3D turbulent annular swirling decaying flow induced by means of a tangential inlet. Exp. Fluids, 29: 291-301.

Rajendran, R. and K. Narasimhan, 2006. Deformation and fracture behaviour of plate specimens subjected to underwater explosion-a review. Int. J. Impact Eng., 32: 1945-1963.

Venturi, D. and G.E. Karniadakis, 2004. Gappy data and reconstruction procedures for flow past a cylinder. J. Fluid Mech., 519: 315-336.